A Solution NMR Molecular Model for the Aspartate-Ligated, Cubane Cluster Containing Ferredoxin from the Hyperthermophilic Archeaon *Pyrococcus furiosus*†

Simon Sham,‡ Luigi Calzolai,‡ Peng-Liang Wang,‡ Kara Bren,‡ Halvard Haarklau,‡ Philip S. Brereton,§ Michael W. W. Adams,§ and Gerd N. La Mar*,‡

Department of Chemistry, University of California, Davis, California 95616, and Department of Biochemistry and Molecular Biology, Center for Metalloenzyme Studies, University of Georgia, Athens, Georgia 30602

Received May 9, 2002; Revised Manuscript Received July 24, 2002

ABSTRACT: A solution molecular model for the conformationally dynamically heterogeneous *Pyrococcus furiosus* ferredoxin with an intact disulfide bond has been constructed on the basis of reported ^{1}H NMR spectral parameters using distance geometry and simulated annealing protocols. Conventional long-mixing time NOESY and H-bonding constraints have been augmented by previously reported short-mixing time NOESY, steady-state NOE, and cluster paramagnetism-induced relaxation. The family of 15 structures with inconsequential violations exhibited low rms deviations for backbone atoms for the overwhelming majority of the residues, including the cluster ligating loop with the unprecedented ligated Asp14. Larger rms deviations were observed across the disulfide bond, but closer inspection revealed that the 15 structures can be factored into 10 substructures exhibiting an "*S*" or right-handed disulfide orientation and 5 exhibiting an "*R*" or left-handed disulfide orientation. The remainder of the structure is indistinguishable for the two disulfide orientations but confirms stabilizing extensions of secondary structural elements in the lengthening of the long helix and both the lengthening and incorporation of a third strand into the β-sheet involving the termini, with these extensions interacting strongly in a modular fashion through the rings of Tyr46 and Trp2. These extensions of stabilizing interactions in *Pyrococcus furiosus* Fd, however, lead to strong destabilization of the disulfide bond and destabilization of the highly conserved first and last β-turns in the sequence. It is concluded that the structural alternations in *Pyrococcus* Fd relative to other hyperthermostable Fds are not to increase thermostability but to place "stress" on the disulfide bond and render it more reducible. The possible physiological implications of this unique reducible disulfide bond are discussed.

The bacterial-type ferredoxins (Fds)[1] are small electron-transfer proteins that possess cubane 4Fe:4S and/or 3Fe:4S clusters attached to the protein matrix by Fe ligation of Cys via a conserved consensus ligating sequence (*1*−*4*). The four ligating residues in a single cluster containing Fd are labeled **I**−**IV** as shown in Figure 1 for the sequence alignment for three Fds of interest. The other two Cys, labeled **V** and **VI**, form a disulfide bond. Iron−sulfur cluster proteins are currently of significant interest in the context of the magnetic properties of the cluster(s) (*5*, *6*), protein control of redox potential (*7*−*10*), and the elucidation of the structural basis of hyperthermostability (*11*−*26*). The Fd protein sequences are highly homologous (*1*), and crystal (*13*, *27*, *28*) or solution NMR (*17*, *18*, *21*, *29*, *30*) structures have been reported for several single cluster (*13*, *27*−*29*) and two-cluster Fds (*12*, *14*, *31*, *32*). The structures of single and double cluster Fds are remarkably similar among members of each class even for Fds with very different thermostability. One single cluster Fd, that from the hyperthermophilic archeaon *Pyrococcus furiosus* (*Pf*), possesses several properties (*33*) that distinguish it not only from Fds from mesophiles but also from Fds of other hyperthermophiles. The sequence of *Pf* Fd is compared in Figure 1 with that of two other structurally characterized single cluster Fds from hyperthermophiles, that of the archeaon *Thermococcus litoralis* (*Tl*) (*34*, *35*) and the bacterium *Thermotoga maritima* (*Tm*) (*13*, *18*). While *Tl* and *Tm* Fds exhibit not only strong sequence, and hence structural, homology to Fds from mesophiles, *Pf* Fd possesses an Asp (Asp14) in position **II** of the consensus ligating sequence (which ligates the cluster in all four-iron cluster oxidation states) (*36*). The electron self-exchange rate for *Pf* Fd is retarded by a factor $\sim 10^3$ relative to Fds from either mesophiles or other hyperthermophiles, and this difference is abolished by the single Asp14 → Cys mutation (*37*).

Pf Fd, in contrast to the other hyperthermostable Fds, exhibits a readily reducible disulfide bond (*38*). This disulfide bond is cleaved at about the same potential as the 4Fe cluster, although the kinetics of thiol formation have not been studied with donors of potential metabolic relevance. Indeed, the

† This research was supported by grants from the National Science Foundation, MCB 96-00759 (G.N.L.) and MCB 99-04624 (M.W.W.A).

* Corresponding author. Phone: (530) 752-0958. Fax: (530) 752-8995. E-mail: lamar@indigo.ucdavis.edu.

‡ University of California.

§ University of Georgia.

[1] Abbreviations: *Pf*, *Pyrococccus furiosus*, *Tm*, *Thermatoga maritima*; *Tl*, *Thermococcus litoralis*; Fd, ferredoxin; NMR, nuclear magnetic resonance; NOESY, two-dimensional nuclear Overhauser spectroscopy; NOE, nuclear Overhauser effect; rmsd, root-mean-square deviation; TOCSY, two-dimensional total correlation spectroscopy; MD, molecular dynamics.

10.1021/bi020347+ CCC: $22.00
Published on Web 09/18/2002

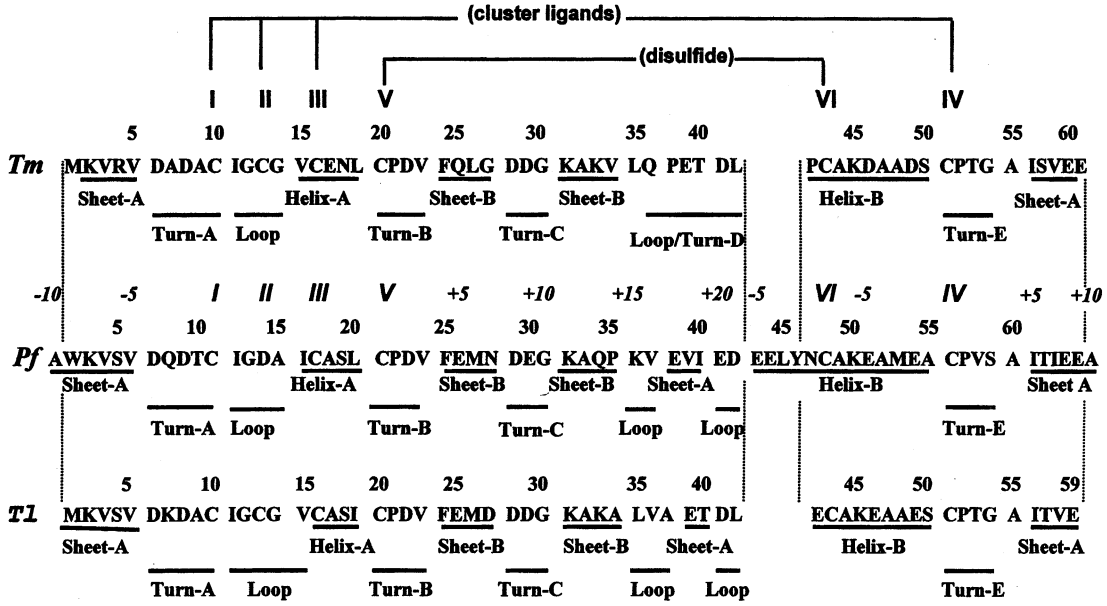

FIGURE 1: Comparison of sequences and secondary structural elements of *Pf* Fd with those of the structurally characterized, hyperthermostable *Tm* (*13*) and *Tl* (*21*) Fds. The roman numerals represent the cluster ligating residues **I**−**IV** and the two Cys that participate in the disulfide bond (**V**, **VI**). Positions ***I***, ***III***, and ***V*** provide convenient reference points for comparing the structures involving residues through Asp42-(***V***+*21*) in *Pf*, while position **VI** is the reference point for describing residues Glu43(**IV**−*13*) to Ala66(***VI***+*10*) in the three structures. This labeling scheme is shown in italics between the *Pf* and *Tm* Fd sequences.

physiological significance of the reducible disulfide bond is not yet understood. *Pf* Fd also exhibits small sequence extensions of the termini, as well as an insertion of four residues, relative to other Fds (see Figure 1), which have been proposed to lengthen the long helix by one turn and the β-sheet in *Pf* relative to all other characterized cubane Fds (*19*, *20*). Last, all forms of WT and cluster−ligand mutated *Pf* Fd derivatives with an intact disulfide exhibit a dynamic equilibrium heterogeneity (*19*, *20*, *39*) that has been proposed to originate from population of alternate (*R*- or left-handed and *S*- or right-handed) $C_\beta-S-S-C_\beta$ orientations of the disulfide bond (*20*). Structurally characterized single cluster Fds with Cys **V** and Cys **IV** form a disulfide bond exclusively with the *S*-orientation (*13*, *18*, *21*, *27*).

Neither the retarded electron-transfer rate (*37*) nor the ready reducibility of the disulfide bond (*38*) in *Pf* Fd lends itself to interpretation based on the conventional and highly conserved cubane Fd structure (*13*, *18*, *21*, *27*−*30*). Thus the absence of a suitable molecular model hampers effective strategies for modulating via mutagenesis these unusual properties of *Pf* Fd. Initial efforts to secure *Pf* Fd crystals suitable for X-ray crystallography were unsuccessful. The recent crystallographic characterization of the *Pf* 4Fe Fd_A^{ox} [ox superscript indicates oxidized cluster and subscript A indicates an intact Cys21(**V**)−Cys48(**VI**) disulfide bond (*38*)] in a 1:1 complex with its redox partner aldehyde oxidoreductase (AOR) revealed a well-resolved cluster, but this was within the part of the Fd that was in contact with AOR, and the remainder of the Fd was lost due to disorder (*40*). It is likely that this structural disorder in the crystal is related to a dynamic equilibrium heterogeneity detected by NMR (*19*, *20*, *39*). In the absence of a crystal structure, a solution NMR-based molecular model has been pursued (*19*, *20*, *41*). Recent results indicate that relatively robust complete solution structures can be derived from cubane cluster Fds (*5*, *14*, *18*, *21*, *29*, *30*, *42*, *43*) (as well as the related high-potential iron−sulfur protein) (*5*, *42*). The necessary assignments both remote from (*19*, *20*) and close to[2] (*41*) the paramagnetic cluster have been made, and sufficient dipolar contacts (NOEs) and paramagnetic-induced relaxation rates[2] (*41*) have been observed to allow the construction of at least a preliminary model of *Pf* Fd. Similarly, extensive NMR data (*20*) on the readily prepared *Pf* 3Fe Fd_A^{ox} (and less extensive data on the mutant *Pf* 4Fe D14C-Fd^{ox}) indicate negligible structural change away from the cluster upon extraction of one iron from the cluster [or the mutation of the cluster ligand Asp14(II)→Cys]. Some dozen residues of *Pf* 4Fe Fd^A_{ox} (as well as *Pf* 3Fe Fd_A^{ox} and D14C-Fd_A^{ox}) exhibited severe line broadening of their NH resonances such that relatively few NOEs were observed to these NHs (*20*). However, the absence of NOEs for these NHs may not be a serious disadvantage, since they likely reflect the average over the two interconverting structures (see below).

We report herein on a preliminary molecular model for *Pf* 4Fe Fd_A^{ox} based on constraints obtained from slow repetition rate, long-mixing time NOESY that characterize the region remote (R_{Fe} >6 Å) from the cluster[2] (*19*, *20*, *41*), rapid repetition rate, short-mixing time NOESY that provide crucial dipolar contacts for protons closer than 6 Å from the iron, steady-state NOEs connecting the strongly relaxed but hyperfine-shifted cluster ligands to the protein matrix (*36*, *41*), and paramagnetic-induced relaxation times for protons <6 Å from R_{Fe} (R_{Fe} is the distance to the nearest cluster iron)[2] (*41*, *44*). The resulting model provides support for a conformational equilibrium for the disulfide bond where the conventional *S*- or right-handed disulfide bond and a generally conserved turn are both destabilized by extensions of the long helix and β-sheet involving the termini via the novel strong interaction of a pair of aromatic rings on those extensions of secondary structure. The possible physiological

[2] L. Calzolai, H. Harklau, P. Brereton, M. W. W. Adams, and G. N. La Mar, submitted for publication.

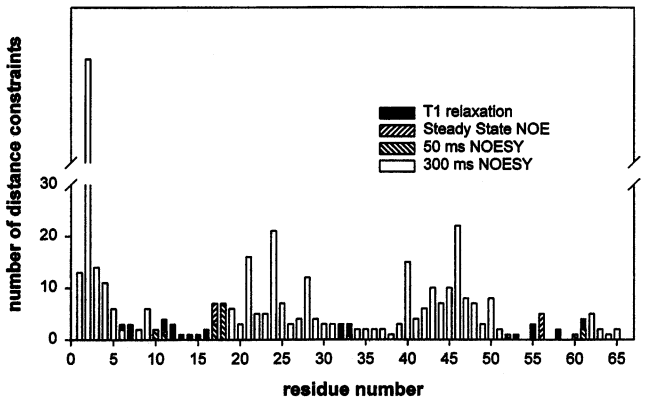

FIGURE 2: Schematic representation of the number, distribution, and nature of the structural constraints available for the solution structure determination of *Pf* Fd.

relevance of the disulfide, which is consequently readily reducible, is discussed.

EXPERIMENTAL PROCEDURES

Source of Protein and NMR Spectroscopy. Growth of *P. furiosus* and purification of the 4Fe Fd were carried out as described (*45*, *46*). NMR analyses and the spectral parameters from 1D and 2D NMR data have been described in detail previously[1] (*20*, *36*, *41*).

Distance Constraints from NOEs. The majority of the distance constraints were obtained from 300 ms mixing time NOESY spectra at 30 and 40 °C which reflect interproton distances remote from the cluster (*20*). Cross-peak intensities were calibrated as strong, medium, and weak to correspond to interproton distance ranges of <2.5, 2.5−3.5, and 3.5−5.0 Å, respectively. In cases where stereospecific assignments were not available, distances were adjusted accordingly to the pseudoatom position. A total of 338 constraints [11 intraresidue, 127 sequential, 69 intermediate range (i+2, i+4), and 131 long range] were obtained from the 300 ms map.

The proximity to the cluster of numerous protons, and their resultant enhanced relaxation, will suppress NOESY peak development involving such protons (*47*). Hence, the distance constraints for cross-peaks involving protons which the resulting molecular structure placed <6 Å from an iron were derived using a 50 ms NOESY map as previously discussed in detail (*21*). In the immediate vicinity of the cluster, in particular for spatial constraints to ligated residues, distance constraints were derived from steady-state NOEs, η_{ij}, for which distances were obtained from the magnitude of the NOEs and estimates of the T_1 for the detected NOE via $\eta_{ij} = \sigma_{ij}T_{ij}$, where $\sigma \propto r_{ij}^{-6}$, with $\sigma = 3\ s^{-1}$ for a methylene group ($r_{ij} \sim 1.8$ Å). The distributions of the various NOE constraints are summarized at the bottom of Figure 2. The individual constraints are listed in Supporting Information.

Relaxation Constraints. Protons near the cluster with $R_{Fe} > 4.5$ Å, $T_1 > 10$ ms, are relaxed by the cluster paramagnetism according to the relation (*41*, *48*, *49*) $T_{1i}^{-1} = D\sum_{q=1}^{4} R_{Fe_q-I}^{-6}$, where R_{Fe_q-I} is the distance of proton i from Fe_q in the 4Fe cluster. The derivation of distance constraints from T_1 relaxation data in this work was discussed in detail previously (*21*). The distribution of relaxation constraints among the residues in *Pf* Fd is included in Figure 2, and the individual constraints are listed in Supporting Information.

Other Constraints. A disulfide bond is formed between Cys21 and Cys48 on the basis of both sulfhydryl titration (*38*) and local NOESY cross-peak patterns. Hydrogen bond constraints were introduced for the slowly exchanging peptide NH identified previously (*19*, *20*) by examination of the NOESY cross-peak pattern to indicate the likely acceptor oxygen; distance ranges involving these likely hydrogen bound NH−O were set at 1.9−2.5 Å.

Structural Modeling of Pf Fd. All structural calculations of *Pf* Fd were performed using the NMR-Refine and Discover software packages (San Diego, CA) operating on a Silicon Graphics Octane workstation, as reported previously for *Tl* 4Fe Fd (*21*). Due to the electron delocalization, the partial charges for the Fe and S atoms in the cluster were used instead of using their formal charges in the calculations. The geometry and partial charge parameters for a [4Fe-4S] cluster were used as those reported previously (*8*) with the exception of one of the cluster Fe atoms which is ligated to Asp14 Oγ. To our knowledge, the determination of the geometry and partial charges of a [4Fe-4S] cluster in a similar model system has not been reported. Therefore, the partial charge of the Fe atom ligated to Asp Oγ was "tentatively" assigned a value of +0.6, which is slightly higher than that of the other Fe atoms (+0.4) in the cluster.

An initial extended structure of *Pf* Fd was built and then used to generate a total of 100 embedded structures in distance geometry (DG) calculations. The embedded DG-generated structures were minimized with 500 steps of steepest descent and 300 steps of conjugate gradient to remove any close contacts in the embedded structures before proceeding to the restrained simulated annealing molecular dynamics (MD) calculations in Discover 2.95. During MD calculations, peptide dihedral angels, ω, were forced to a trans configuration for all residues with four prolines. A nonbonded cutoff distance of 5 Å was used. No cross and charged terms were included in the calculations. A total of eight phases with a total simulation time of 65 ps were used in restrained MD simulations. At the beginning, all of the force constants for bonded, NOE, and nonbonded interactions are scaled down from their full values. During the first three phases of restrained MD calculations, the embedded structures were subjected to simulation for a total of 50 ps at 1000 K. By the end of the third phrase, the force constants for bonded and NOE interactions were scaled back to their full values while that of nonbonded interaction was scaled back to 20% of its full value only. The last three phases consist of restrained MD from 700 K → 500 K → 300 K with a 5 ps simulation time at each phase. The force constant for nonbond interaction was gradually scaled back to its full value at the last phase. The calculated structures were then minimized with 1000 steps of steepest descent and 2000 steps of conjugate gradient methods. To make sure the structures were calculated correctly, the structures were checked and corrected periodically according to the procedures described in detail previously for *Tl* 4Fe Fd (*21*).

Finally, a total of 15 structures with minimal numbers of constraint violations and without NOE constraint violations >0.4 Å were retained. The overall quality of these refined structures was examined with the program PROCHECK. The Ramachandran plot for the structures is shown in Supporting Information. With the exceptions of Gln8 and Pro35, the majority of backbone ϕ/ψ dihedral angles reside in the well-

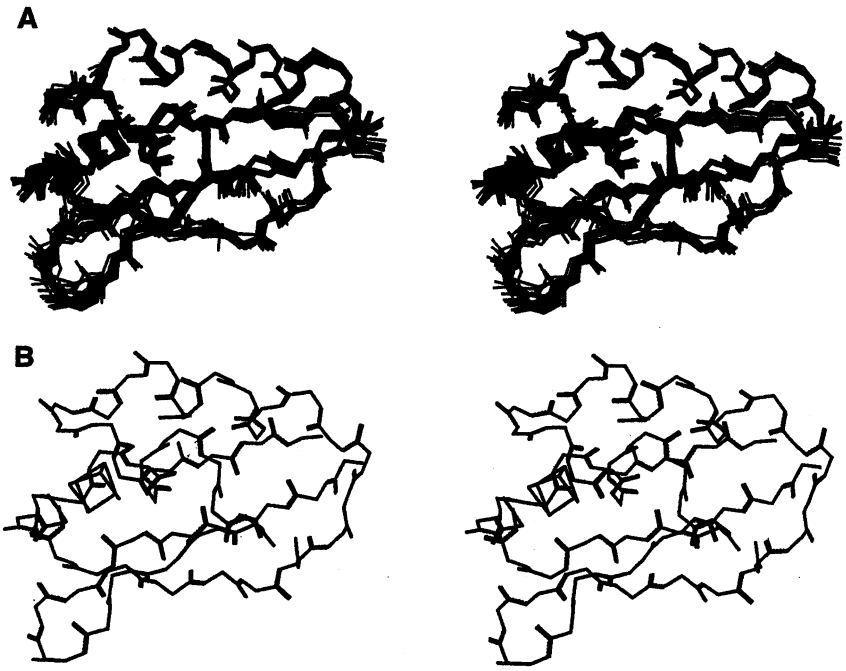

FIGURE 3: Stereoviews of the superposition of backbone atoms of the 15 accepted *Pf* Fd NMR structures with minimal constraints and (B) backbone atoms from the crystal structure of *Tm* Fd (*13*).

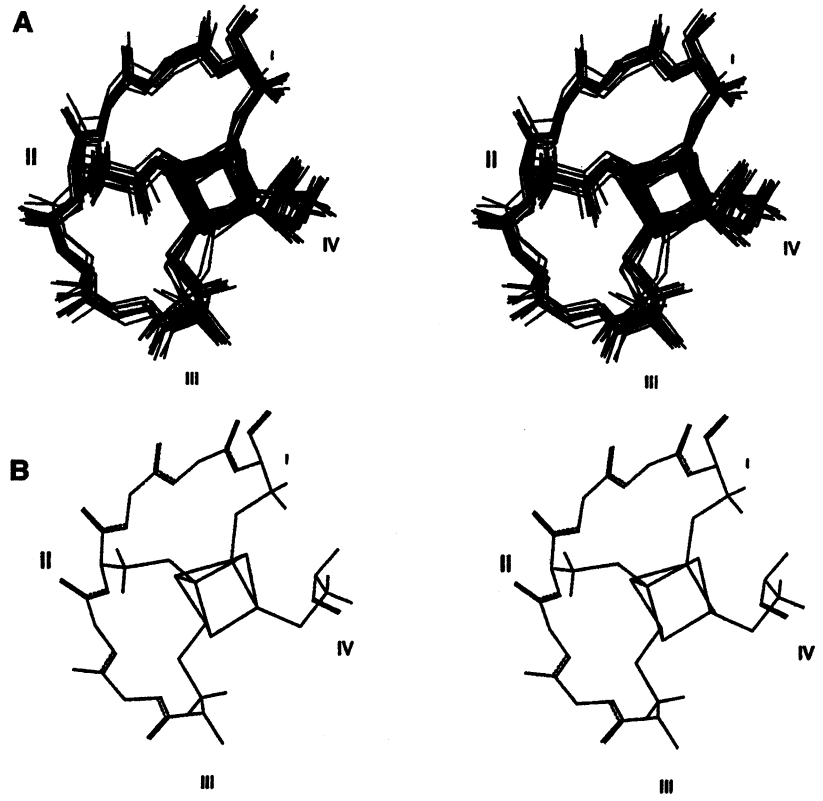

FIGURE 4: Stereoviews of an expansion of Figure 3 to focus on the backbone atoms for the cluster environment [Cys11(**I**)−Cys17(**III**) and Cys**IV**] for (A) the 15 accepted NMR structures of *Pf* Fd and (B) the crystal structure of *Tm* Fd (*13*).

defined, generally acceptable, regions of the Ramachandran plot.

RESULTS

Quality of the Structure. The superposition of the main chain backbone atoms of the 15 structures with only minimal violations is shown in Figure 3A, with the cluster environment expanded in Figure 4. The root-mean-square deviation (rmsd) values of the backbone atoms are shown in Figure 5A. Thus the structures bundle well and yield rmsd values for backbone atoms comparable to those of other cubane Fd NMR-based models (*14*, *18*, *21*, *29*, *30*). The number of constraints used is shown schematically in Figure 2, and the detailed constraints are listed in Supporting Information. The use of short-mixing time NOESY, steady-state NOEs, and T_1s provided the majority of the limited number of constraints

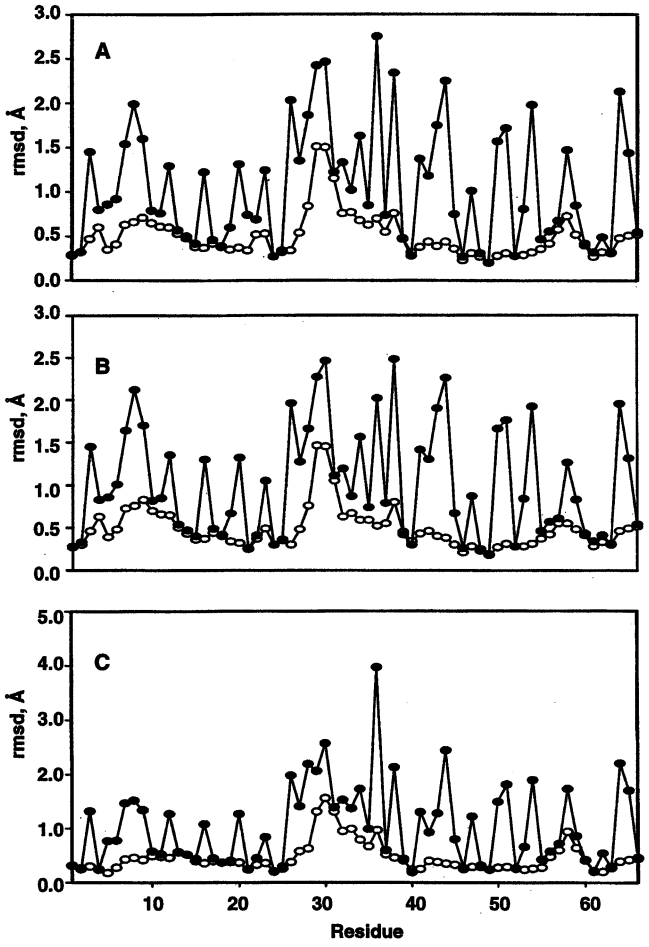

FIGURE 5: Root-mean-square deviation (rmsd) as a function of residue number for the main chain (open markers) and side chain heavy atoms (closed markers) for (A) the 15 accepted *Pf* Fd NMR structures, (B) 10 of the 15 accepted structures with the *R*- or left-handed disulfide bond, and (C) the remaining 5 of the 15 structures with the *S*- or right-handed disulfide orientation.

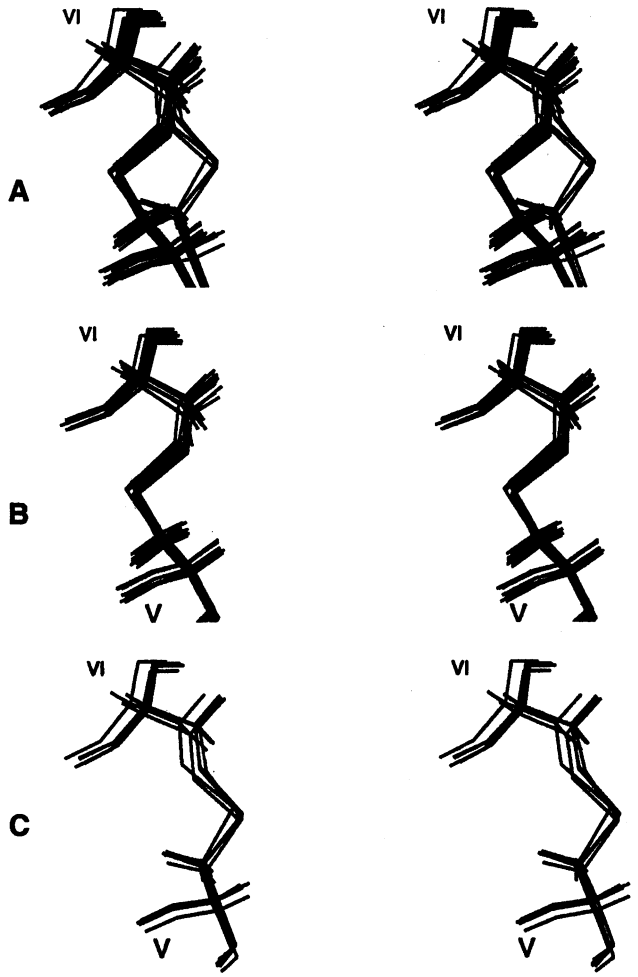

FIGURE 6: Stereoviews of the expansion of Figure 3 showing the superposition of the heavy atoms in the disulfide bond of *Pf* Fd in (A) the 15 accepted NMR structures, (B) 10 of the 15 accepted NMR structures with an *R*- or left-handed disulfide bond, and (C) 5 of the 15 accepted NMR structures with an *S*- or right-handed disulfide orientation.

for residues in the immediate vicinity of the cluster but yielded superpositions, as shown in Figure 3, with rmsd values near the cluster essentially the same as for the majority of the other backbone atoms (Figure 5A). Hence the residual paramagnetism of the cluster does not seriously interfere with the definition of the cluster geometry, as found in other single cubane cluster Fds (*18*, *21*, *29*, *30*) and Hipips (*6*, *42*, *43*). The rmsd values of other heavy atoms are well-defined for residues oriented toward the interior of the molecule (Figure 5A), but those oriented toward the solvent exhibit a distribution of positions with resulting larger rmsd values, as observed in other Fd NMR structures.

The general outline of *Pf* Fd in Figure 3 depicts a molecule with essentially the same secondary structural elements as found previously for single cubane cluster Fds from either mesophiles (*27*, *30*) or hyperthermophiles (*13*, *21*) (*Tm* and *Tl* Fds shown in Figure 1B,C). The same stereoview for the *Tm* Fd crystal structure (*13*) and the present *Pf* Fd NMR model can be compared in Figure 3. The sequence extensions in *Pf* relative to *Tm* or *Tl* Fd manifest themselves simply as extensions of conserved secondary structural elements. However, the details of the secondary structural elements and the interaction among them exhibit some systematic and significant differences from other Fds that are likely related to the unusual functional properties of *Pf* relative to *Tm* Fd or *Tl* Fd.

To effectively analyze the *Pf* Fd structure, it is convenient to convert to a notation for the position of a residue in the sequence such that homologous residues reside in the same structural environment in the three Fds to be compared. Such a system refers to sequence position, in italics, relative to one of the conserved Cys **I**, **III**, **IV**, and/or **V** (i.e., helix A consists of residues ***I***+*5* to ***III***+*3*, β-sheet B consists of residues ***V***+*4* to ***V***+*7* and ***V***+*11* to ***V***+*14*, etc.). This labeling scheme is shown in italics above the sequence of *Pf* Fd in Figure 2. This labeling scheme greatly facilitates comparison of the differences and similarities between *Pf* and *Tm* Fds (which is essentially the same as *Tl* Fd).

Molecular Heterogeneity and the Disulfide Bond. While the main chain atoms in the 15 superimposed structures in Figure 3 yield acceptable rmsd values that are typical for other NMR-based Fd models (*14*, *18*, *21*, *29*, *30*), the rmsd for the $C_\beta-S-S-C_\beta$ in the disulfide bond are significantly larger (not shown, but see Figure 6A) than for the nearby main chain atoms. The disulfide bond in the superimposed structures in Figure 3 is shown in the expansion of this region in Figure 6A. In fact, the superposition for all 15 structures in Figure 6A suggests two major contributing forms of 10

structures, shown in Figure 6B, and 5 structures, shown in Figure 6C. The conformation in Figure 6C resembles the *S*- or right-handed disulfide bond (*50*) (as observed in all other structurally characterized single cluster Fds) (*13*, *18*, *21*, *27*). The conformation in Figure 6B reflects a structure closer to that expected for the *R*- or left-handed disulfide bond (*50*). The rmsd for the $C_\beta-S-S-C_\beta$ in the resolved superpositions in Figure 6B,C are now comparably low (not shown; see Supporting Information) to those of the nearby main chain atoms. The appearance of disulfide bond orientational isomerism in the computational aspects of our model strongly supports our earlier proposal (*20*) that this isomerism is responsible for two comparably populated interconverting structures of all *Pf* Fd forms that possess an intact disulfide bond.

Factoring the 15 superimposed whole structures in Figure 3A into 10 separately superimposed structures with the *S*-disulfide orientation and the 5 structures with the *R*-disulfide orientation reveals indistinguishable models (not shown; see Supporting Information), in that any slight difference between the two overlaid sets of structures for any one main chain atom represents only a very small fraction of the rmsd for that atom in each of the two bundles of structures. The rmsd values for main chain atoms and all heavy atoms as a function of position for the separately superimposed structures with the *S*-disulfide and *R*-disulfide bond are shown in Figure 5B,C. It is clear that, at the presently attainable resolution, molecular heterogeneity is recognizable with any confidence only in the disulfide bond orientation (see Supporting Information for separate superimpositions of the "*S*"- and "*R*"-structural backbones). Hence the description of the remainder of the structural features of 4Fe *Pf* Fd and comparisons with *Tm* Fd (*13*, *18*) apply equally to both disulfide orientations included in the 15 structures in Figure 3A. The likely hydrogen bonds involving the main chain atoms are identified on the basis of a heteroatom separation of 2.5−3.5 Å and X−H−Y bond angles >100°.

Secondary Structural Elements in Pf Fd. (A) α*-Helices*. *Pf* 4Fe Fd possesses two α helices, a short, one-turn, 5-residue helix A near the N-terminus involving residues Ile16−Leu20 (i.e., residues ***I****+5* to ***III****+3*) that appears identical to the highly conserved helix involving residues ***I****+5* to ***III****+3* in other Fds (*13*, *21*, *27*) (Figure 1). A longer helix is found near the C-terminus. This second helix B exhibits a regular structure with no obvious deformations (see below) but is lengthened by ∼1 turn via the 4-residue insertion Glu44−Asn47 relative to Fds from either other hyperthermophiles (*13*, *21*) (Figures 1B,C) or mesophiles (*27*−*30*). This helix extension results in an additional four backbone H-bonds relative to other Fds, as listed in Table 1.

(B) β*-Sheets*. *Pf* Fd, like other single cluster Fds (*27*−*30*), possesses two antiparallel β-sheets. The small, inner β-sheet B consists of Phe25−Asn28 (residues ***V****+4* to ***V****+7*), and Lys32−Pro35 (residues ***V****+11* to ***V****+14*) is well formed (not shown; see Supporting Information) with the main chain H-bonds homologous to *Tm* Fd (see Table 1). This β-sheet B, in contrast to *Tm* (*13*) or *Tl* (*21*) Fds where the residue (***V****+14*)−residue (***V****+15*) peptide bond is the conventional trans bond, contains the Pro35(***V****+14*)−Lys36(***V****+15*) bond which exhibits a cis peptide orientation. While this places the backbone angle of the Pro into a less favorable portion of the Ramachandran plot (not shown; see Supporting Information), it still allows the robust residue (***V****+14*) (Pro35) to residue Val(***V****+3*) H-bond found in both *Tm* (*13*) and *Tl* (*21*) Fds. The cis Pro35−Lys30 peptide bond may allow an additional H-bond from Asp26 to the Pro35 carbonyl (see Table 1).

The larger β-sheet A in *Pf* Fd, as in other single cluster Fds (*13*, *18*, *21*, *27*−*30*), includes the two termini. The two strands, residues ***I****-10* to ***I****-5* (Ala1−Val6) and ***IV****+5* to ***IV****+10* (Ile61−Ala66), of *Pf* Fd are longer than in either *Tm* or *Tl* Fd (see Figure 1) and, hence, provide two additional backbone H-bonds relative to *Tm* Fd, as listed in Table 1. Earlier qualitative analysis (*19*, *20*) of the backbone NOEs and $C_\alpha H$ chemical shift pattern in *Pf* Fd had suggested that Glu38−Ile40 (residues ***V****+17* to ***V****+19*) form a third strand of β-sheet A. The present model confirms this prediction in that the residues form an extended strand that is superimposable on either the N- or C-terminal strands and leads to the predicted three main chain H-bonds to the N-terminal strand as listed in Table 1.

This β-sheet A makes numerous tertiary contacts with the long helix B, as found in all other single cluster Fds (*13*, *18*, *21*, *27*−*30*). The elongation of both the helix (by four residues) and β-sheet (by ∼1−2 residues) in *Pf* Fd relative to other Fds extends the interaction between these two secondary structural elements in a modular fashion, as is apparent in the comparison in Figure 3. Two key residues on the β-sheet A and α-helix B include the aromatic Trp2 and Tyr46, which have no precedence in other Fds. These two residues constitute the best "resolved" (i.e., very low side chain heavy atom rmsd) of the tertiary contacts in this Fd, with the two rings completely overlapping each other and spaced parallel at the van der Waals separation of ∼3.2 Å, as shown in Figure 7. An interesting consequence of this very strong interaction between the two aromatic rings is that the register of contacts between the β-sheet A and helix B is forced to shift ∼1 Å toward the C-terminus of helix B in *Pf* Fd relative to other Fds (see below) but, in particular, *Tm* Fd, as shown in Figure 7.

(C) Turns. Single cubane cluster Fds generally possess (*13*, *27*−*30*) five β-turns labeled A−E. The generally conserved turn A on the N-terminal side of the cluster involves residues ***I****-4* to Cys**I** (i.e., Asp7 to Cys11 in *Pf* Fd). While such a turn is observed in *Pf* Fd, it appears somewhat deformed from that observed in other Fds, most prominently with ∼180° rotation of the Asp7−Glu8 peptide bond. A conventional β-turn, as in *Tm* Fd (*13*, *18*), leads to the main chain residue ***I****-4* C═O as acceptor to the NHs of residues ***I****-1* and ***I***. In *Pf* Fd, the recognizable backbone H-bonds include Asp7(***I****-4*) C═O as acceptor to the NH of Asp9(***I****-2*) and the Asp8(***I****-3*) C═O as acceptor to the Cys11(***I***) NH (see Table 1). The rotation of the Asp7−Glu8 peptide bond precludes the residue ***I****-1* NH to residue ***I****-4* C═O H-bond observed in *Tm* Fd. That this structural change is likely real is supported by the fact that the Asp7 NH in *Pf* Fd is so labile as to exhibit significant saturation transfer at ambient temperature (*19*, *20*), arguing that it is not involved in an H-bond. Besides these differences, turn A in *Pf* Fd does exhibit the highly conserved tertiary contacts to β-sheet B in the Lys32(***V****+11*) side chain NH H-bonds to the carbonyls of Asp8(***I****-3*) and Cys11(***I***) and to the junction of turn E and β-sheet A in the

Table 1: Proposed Main Chain Hydrogen Bonds in *Pf* Fd and Comparison with Those in *Tm* Fd

	Pf Fd			*Tm* Fd		
position[a]	residues	N···O, Å[b]	N···H···O, deg [c]	residues	N···O, Å[d]	N···H···O, deg [d]
β-sheet A						
I → ***IV***+*10*	A1−A66	3.4	140			
I−*9* → ***V***+*19*	W2−I40	2.9	150	M1−T39[e]	2.77	102
I−*8* → ***IV***+*8*	K3−E64	2.9	140	K2−E59	2.75	164
I−*7* → ***V***+*17*	V4−E38	2.8	140	V3−P37	2.76	170
I−*6* → ***IV***+*6*	S5−T62	3.0	100	R4−S57	3.00	163
V+*18* → ***I***−*9*	I40−W2	3.4	140	T39−M1[e]	2.92	155
IV+*6* → ***I***−*6*	T62−S5	3.1	110	S57−R4	2.99	169
IV+*8* → ***I***−*8*	E64−K3	3.4	150	E59−K2	2.94	167
IV+*10* → ***I***−*10*	A66−A1	2.9	130			
β-sheet B						
V+*5* → ***V***+*13*	E26−Q34	3.4	130	Q25−K33	3.03	154
V+*7* → ***V***+*11*	N28−K32	3.1	130	G27−K31	2.78	152
V+*13* → ***V***+*13*	Q34−E26	3.2	160	K33−Q25	2.72	141
V+*15* → ***V***+*11*	K36−A24	3.4	140	L35−V23	2.77	144
helix A						
III+*1* → ***I***+*4*	A18−A15[2]	4.0	130	E17−G14	3.14	123
III+*2* → ***I***+*5*	S19−A15	3.4	140	N18−G14	3.17	157
III+*3* → ***I***+*4*	L20−I16	3.0	130	L19−V15	3.03	157
helix B						
IV−*10* → ***V***+*21*	Y46−D42	3.1	140	A44−L41	2.99	162
IV−*9* → ***IV***+*3*	N47−E43	2.8	130			
IV−*8* → ***IV***−*12*	C48−Q44	3.1	120			
IV−*7* → ***IV***−*11*	A49−L45	3.0	170	K45−P42	3.14	133
IV−*6* → ***IV***−*10*	K50−Y46	2.7	150			
IV−*5* → ***IV***−*9*	E51−N47	3.4	140	D46−C43[f]	3.26	104
IV−*4* → ***IV***−*8*	A52−C48	3.2	130	A47−C43	2.88	161
IV−*3* → ***IV***−*7*	M53−A49	3.7	150	A48−A44	3.10	152
IV−*2* → ***IV***−*6*	E54−K50	3.8	150	D49−K45	2.95	160
IV−*1* → ***IV***−*5*	A55−E51	3.3	150	S50−D46	2.99	130
turn A						
I−*4* → ***IV***+*4*	D7−A60	3.1	130	D6−A55	2.80	163
I−*2* → ***I***−*4*	D9−D7	3.1	150			
I−*1* → ***I***−*3*				A9−D6	3.02	136
I−*1* → ***I***−*4*	T10−Q8[g]	3.5	90			
I → ***I***−*4*				C10−D6	3.14	139
I → ***I***−*3*	C11−Q8	3.5	140	C10−A7	3.29	127
turn B						
V → ***III***	C21−C17	3.0	150	C20−C16	2.80	141
V+*3* → ***V***	V24−C21	3.2	130	V23−C20	2.91	155
V+*4* → ***III***	F25−C21	3.0	160	F24−C20	2.93	160
turn C						
V+*6* → ***V***+*7*	G31−N28	2.9	150	G30−G27	3.12	151
turn E						
IV → ***III***−*4*				C51−A47	2.98	119
IV+*3* → ***IV***	S59−C56	3.0	110	G54−C51	3.47	157
loop						
V+*16* → ***V***+*3*	V37−A24	3.6	120			

[a] Labeling of residues in the H-bond (donor → acceptor) for residues at homologous positions in the structure using the conserved Cys***I***, ***III***, ***IV***, and ***V*** as reference, as described in Figure 1. [b] Separation between donor (N) and acceptor (O) heteroatoms, in Å. [c] N−H···O bond angle, to nearest 10°. [d] Separation between donor (N) and acceptor (O) heteroatom, in Å, and N−H···O bond, in deg, as taken from the *Tm* Fd crystal structure (*13*). [e] Met1 is not considered as part of β-sheet A; all residues 36−41 are considered as a turn (turn D) in *Tm* Fd (*13*). [f] This hydrogen bond would be of only marginal stability in *Tm* Fd. [g] Despite its favorable hydrogen bond length, the bond angle indicates the presence of a marginally stable H-bond, at best.

main chain H-bond between Asp7(***I***-*4*) peptide NH and the Ala60(***VI***+*4*) carbonyl. The configuration of these conserved H-bonds in *Pf* and *Tm* Fds are compared in Table 1.

Turn B occurs immediately after helix A and constitutes the most strongly conserved portion of the 4Fe Fd structures. Its geometry and H-bonding patterns are unchanged relative to those in either *Tm* (*13*) or *Tl* (*21*) Fd. Turn C connects the two β-sheet B strands and exhibits the largest main chain rmsd. We conclude that this more likely arises from true flexibility of the turn than the lack of sufficient NOESY constraints, since several of its peptide NHs exhibit rapid exchange with solvent. Similar flexibility has been observed in both *Tm* and *Tl* Fds (*49*). The implied H-bonds are listed in Table 1. The conserved turn D in single cubane cluster Fds from mesophiles contains a Pro and makes a single backbone H-bond to β-sheet A. The analogous residue in *Pf* Fd forms the third strand in β-sheet A (*27*, *28*, *30*) (see above). However, this does not introduce additional backbone H-bonds relative to *Tm* Fd. Since the N- and C-terminal residues in *Tm* Fd do not participate in β-sheet A, Met1 aligns with loop/turn D (*13*) (the analogue to the third strand in *Pf* Fd) to provide the analogous third H-bonds to the N-terminal residue as in *Pf* Fd.

Last, turn E in *Pf* Fd results in backbone atom rmsd values (Figure 5) which are not significantly larger than for those from the same turn in other NMR models of single cluster

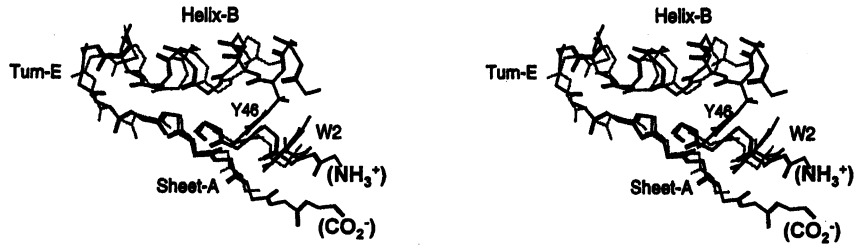

FIGURE 7: Comparison of the average of the 15 accepted NMR structures of *Pf* Fd (dark lines) and the *Tm* Fd crystal structure (light lines) for homologous portions of β-sheet A (N-terminal strand residues ***I*−*9*** to ***I*−*5*** and C-terminal strand residues ***IV*+*5*** to ***IV*+*10***), turn E (residues ***IV*** to ***IV*+*3***), and helix B (residues ***IV*−*9*** to ***IV*−*1***) with optimized superposition for the conserved portion of the C-terminal strand for β-sheet A. Note the shift of helix B toward its C-terminus in *Pf* relative to *Tm* Fd. The change in register between β-sheet A and helix B in *Pf* relative to *Tm* Fd appears to result from the close contacts between the two rings of the unique Trp2 and Tyr46 residues in *Pf* Fd.

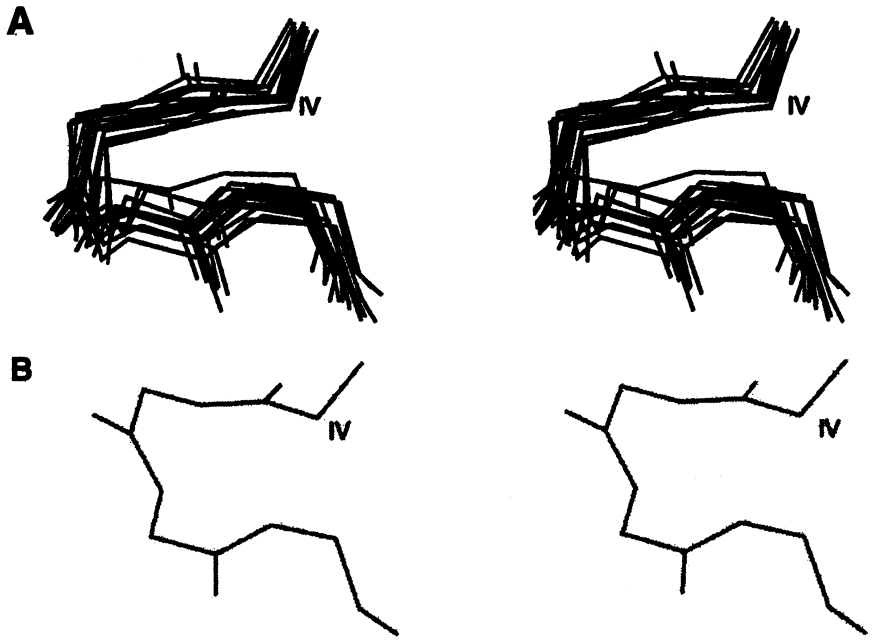

FIGURE 8: Comparison of turn E involving residues ***IV*** to ***VI*+*3*** (Cys56−Ser59 in *Pf* Fd; Cys51−Gly54 in *Tm* Fd) for (A) the superposition of the 15 accepted NMR structures of *Pf* Fd,and for (B) the *Tm* Fd crystal structure (*13*).

bacterial Fds (*21*, *29*, *30*). However, as shown by the portion of the superimposed 15 structures that include residues Cys56(***IV***)−Ser59(***IV*+*3***) (see Figure 8A), turn E is significantly perturbed with respect to its highly conserved structure (see Figure 8B) in *Tm* (*13*) and *Tl* (*21*) Fds, as well as in mesophilic cubane Fds (*29*, *30*). The perturbation basically reflects a conversion from a trans to a cis peptide bond for the Ser59−Ala60 linkage in each of the 15 structures. Possible structural bases for this deformation of turn E are considered below.

(D) Loop between β-Sheets A and B. Residues Cys21, Val24, Lys36, and Val37 exhibit NH resonances that are severely broadened by the dynamics equilibrium between the *S*- and *R*-disulfide bridge (*20*). The NHs of residue ***V*+*15*** (Lys36 in *Pf*) and the highly conserved Val24(***V*+*3***) serve as H-bond donors to the carbonyls of the conserved Cys(***V***) and Val(***V*+*3***) (see Supporting Information) in both *Pf* (Cys21, Val24) and *Tm* (*13*) (Cys20, Val23) Fds (Table 1). In *Pf* Fd, unlike the *Tm* protein, residue ***V*+*16***(Val37 in *Pf* Fd) appears to serve as a weak H-bond donor to Val(***V*+*3***) (Table 1). This confirms that the four residues whose NH chemical shifts are most strongly differentiated for the alternate orientations of the *S*- and *R*-disulfide bond (*20*) are present in a single 4-residue H-bond chain that links the cluster to β-sheet A. The present structure does not shed light on what the alternate structures are for these residues for the *R*- and *S*-disulfide orientations. The only evidence, albeit weak, for structural heterogeneity in the link between β-sheets A and B is that residues Lys36 and Val37 exhibit somewhat larger rmsd values than nearby main chain atoms.

The Fe−S Cluster. The structure of the cluster is determined (see Figure 4) to the same precision as is the majority of the remainder of the structure for which considerably more constraints are available (Figure 2). The well-defined main chain positions for residues Cys***I***−Cys***III*** in *Pf* Fd are not detectably altered from those found in, for example, *Tm* Fd (*13*), as shown in the comparison in Figure 4. The *Pf* Fd structure, moreover, reveals Cys11(***I***), Cys17(***III***), and Cys56(***VI***) orientations (χ_2) that are essentially conserved relative to those found for the homologous Cys in *Tm* (see Figure 4) or *Tl* 4Fe Fds (*13*, *21*). These results are consistent with the observation of similar patterns of Cys $C_\beta H$ contact shifts and/or relaxation rates in *Pf* (*36*) and *Tl* (*21*, *49*) or *Tm* 4Fe Fd, both of which depend strongly on Fe−S−C_β−H angles (*6*, *42*, *51*, *52*). The unique Asp14(***II***) in *Pf* Fd is found with a well-defined orientation in the 15 superimposed structures (see Figure 3) with the same $C_\alpha H$ position relative to the cluster as found for the Cys***II*** $C_\alpha H$ in *Tm* Fd, despite

Table 2: Proposed H-Bonds to Cluster Ligands in *Pf* Fd and Comparison with Those in *Tm* Fd

	Pf Fd			*Tm* Fd		
position[a]	residues	N···S(O), Å[b]	N···H···S(O), deg[c]	residues	N···S(O), Å[d]	N···H···S(O), deg[d]
I*+2 → *S2	I12−S2	3.9	160	I11−S2	3.30	161
I*+2 → *I	G13−C11	4.1	120	G12−C10	3.36	148
***I*+2 → *I*+3**	G13−D14(O)	4.2	140			
I*+4 → *S1	A15−S1	3.4	130	G14−S1	3.26	155
***I*+5 → *I*+3**	I13−D14(O)	3.3	150	V15−C13	3.50	171
III* → *S4	C17−S4	3.5	140	C16−S4	3.56	134

[a] Labeling of residues in the H-bond (donor → acceptor) for residues at homologous positions in the structure using the conserved Cys***I***, ***III***, ***IV***, and ***V*** as reference, as described in Figure 1. [b] Separation between donor (N) and acceptor S (O) or heteroatoms, in Å. [c] N−H···S(O) bond angle, to nearest 10°. [d] Separation between donor (N) and acceptor S(O) or heteroatom, in Å, and N−H···S(O) bond, in deg, as taken from the *Tm* Fd crystal structure (*13*).

providing no constraints to the structure determination. Hence the ligated Asp14(***II***) appears not to perturb the conformation of the consensus ligating sequence, Cys(***I***)XXAsp(***II***)XXCys-(***III***), relative to the more conventional one with a Cys(***II***).

The H-bonds to cluster−ligand side chains or bridging sulfide atoms are identified by the position of labile protons relative to potential acceptors. There are 10 likely H-bonds to the cluster, and these, with two exceptions, are conserved in both number and location relative to *Tm* Fd (*13*), as shown in Table 2. The trans to cis conversion of the Ser54−Ala60 peptide bond in turn E of *Pf* Fd eliminates the possibility of the Cys***VI***(56) NH to Val58 to S H-bond. However, it appears as if the Gly13(***I*+2**) NH serves as H-bond donor to the ligated carboxylate oxygen of Asp14(***II***), leading to the same number of H-bonds to cluster atoms.

The present molecular model for the cluster does not shed any light on a structural basis for the strong retardation of the electron self-exchange rate (*37*) in the WT Asp14(***II***) ligated versus the mutant Cys14(***II***) ligated in the 4Fe form of *Pf* Fd. However, one possibility, that the Asp14(***II***) provides bidentate in one, and monodentate cluster ligation in the other, oxidation state, cannot be discounted. Investigation into whether, in fact, the Asp14(***II***) chelates the iron in one of the two-cluster oxidation states has not been explored, and such studies warrant both more extensive assignments on a $^{15}H/^{13}C$-labeled sample as well as a study of the optimized charges pertinent to both monodentate and bidentate Asp ligation.

Structural Implication for Hyperthermostability. There is strong current interest in elucidating the structural basis of hyperthermostability in proteins (*11*, *13*, *23*−*26*). Because of their small size and monomeric nature, bacterial Fds (*12*−*14*, *18*−*21*), like their related single-iron rubredoxins (*11*, *15*, *53*), have provided important insight into the remarkably small and widespread structural differences in iron−sulfur cluster proteins from hyperthermophiles and mesophiles. Inspection of the main chain H-bonds in Table 1 reveals a significant increase in number for the Fd from *Pf* (T_{opt} 100 °C) (*54*) relative to that from *Tm* (T_{opt} 80 °C) (*55*).

Unfortunately, however, *Pf* Fd does not appear to be a suitable candidate for shedding light on the structural basis for the unusual thermostability of this protein. There are at least two reasons for this conclusion. On one hand, the present model is only preliminary and represents an "average" structure for the two interconverting disulfide orientations (*20*, *39*) for which the extent of structural differences away from the disulfide bond is currently unknown. On the other hand, and likely more importantly, even the current preliminary molecule model of *Pf* Fd clearly shows that, in comparison to both hyperthermostable *Tm* (*13*, *18*) and *Tl* (*21*) Fds, as well as Fds from mesophiles (*27*), while several structural features are stabilized relative to all other Fds (i.e., inclusion of the third strand in β-sheet A, increased length of helix B and β-sheet A, and their strong interaction via Trp2 and Tyr46), other generally conserved structural features (i.e., turns A and E, disulfide bond, several cis peptide bonds) are destabilized relative to the same Fds. While a systematic comparison has not been reported, it has been proposed that *Tm* and *Pf* Fds exhibit quite similar stabilities at high temperatures (*16*). This suggests that the additional stabilizing and destabilizing interactions essentially cancel in *Pf* relative to *Tm* Fd.

Structural Implication for Disulfide Reducibility. The most significant difference in physicochemical properties between *Pf* Fd and the other two structurally characterized hyperthermostable Fds is the ready reducibility of the disulfide bond, which is cleaved in *Pf* Fd at about the same potential as the cluster (*38*). The unprecedented ligation of the cluster by one Asp14(***II***) (*36*) somewhat perturbs the reduction potential (−368 mV) relative to the *Pf* D14C-Fd (−426 mV) to that more comparable to the values reported for the majority of all-Cys ligated Fd clusters (∼−400 mV) (*46*). The present structural model serves to confirm our previous proposal (*20*) that the disulfide bond is destabilized by the extension of helix B by one turn toward the N-terminus, which places Cys(48)***VI*** on the center of a helix. This position is expected to lead to destabilization of the disulfide because of unfavorable steric interaction of the Cys***VI*** Sγ with the helix backbone in both the favored traditional *S*-orientation or the less favored *R*-orientation (*50*). A correlation between the tendency to populate the less-favored disulfide *R*-orientation with reducibility at the disulfide has been noted previously (*56*, *57*).

Turn E is destabilized in *Pf* Fd because of the trans to cis rotation of the Ser59−Ala60 bond, but its potential effect on disulfide reducibility is not clear. A logical link between this deformation of turn E can be rationalized on the basis of other unique properties of the protein. A particularly significant and strong tertiary contact exists in *Pf* Fd between the unique Trp2 ring and that of the Tyr46 on the 4-residue insertion that lengthens helix B. The backbone segment of the protein involving helix B (residues ***IV*-*8*** to ***IV*-1**), turn E (residues ***IV*** to ***IV*+*3***), and the C- and N-terminal strands of β-sheet A (residues ***I*-*5*** to ***I*-*10***) for *Pf* and *Tm* Fds are shown in the stereoviews in Figure 7 where the extended β-strands of β-sheet A are superimposed. It is clear from

this comparison that the specific and strong interaction between the Trp2 and Tyr46 rings results in a change in the register of the helix B to β-sheet A tertiary contacts, in that the β-sheet strand is translated by ~1 Å toward the N-terminus in *Pf* relative to *Tm* (or *Tl*) Fds. Since both helix B and the N-terminal strand exhibit the regular structure for their respective secondary structural elements, their shift in the register of helix B to β-sheet A tertiary contacts must be accommodated by the connecting link between helix B and the C-terminal strand of β-sheet A, namely, turn E. It is reasonable to expect that substitution of either one or both of the aromatic rings of residues 2 and 46 by bulky aliphatic side chains (i.e., Leu) would lead to, among other changes, a restoration of a "normal" β-turn for turn E, as is found in the other hyperthermophilic Fds (*13*, *18*, *21*).

The most likely link between the destabilization of turn E and the disulfide bond could occur if the disulfide bond indeed deforms helix B in one or both of the two interconverting forms with the alternate disulfide orientations. While only a regular, undeformed, but "averaged", helix B is observed, very large line broadening of helix B peptide NHs for Lys50, Ala52, and Glu54 due to interconverting *S*- and *R*-disulfide orientations (*20*) indicates that disulfide stereochemistry obviously strongly perturbs at least the strength of the H-bonds within the helix. However, the influence of replacing the aromatic ring(s) (by site-directed mutagenesis) on disulfide reducibility would first have to be ascertained before proposing a specific structural relationship. Connection between the conversion of the more stable trans peptide bond in *Tm* Fd to cis in *Pf* Fd for residues in turn A [Asp7(***I****-4*)−Gln8(***I****-3*)] and in the loop that connects β-sheets A and B [Pro35(***V****+14*) to Lys36(***V****+15*)] and disulfide reducibility are obscure at this time. The additional residues in *Pf* relative to *Tm* and *Tl* Fds are therefore not present to further stabilize *Pf* Fd relative to other Fd. Rather, they are present to generate an "entatic" state (*58*), where the global molecular structure places "strain" on a chromophore that "drives" the molecule a portion up the reaction pathway toward disulfide bond cleavage.

The fact that secondary structure has such a direct influence on the properties of the disulfide bond lends credence to the notion that *Pf* Fd has a specific role in thiol interconversions that are metabolically relevant. Direct interactions between FeS centers and disulfides, including both homo- and heterodisulfides and both inter- and intramolecularly, have recently been shown to play key roles in a variety of biological processes (*59*−*61*). However, as yet, these do not involve intramolecular electron transfer in what is ostensibly a "conventional" Fd like the *Pf* protein. In fact, this Fd is already known to play a central role in the primary metabolism of *Pf*, and many Fd-linked oxidoreductase enzymes involved in carbon and nitrogen metabolism have been characterized (*62*). These include an NADH:Fd oxidoreductase, which allows communication between one- and two-electron carriers within the cell (*62*). It is therefore not clear how the ability of *Pf* Fd to donate two electrons via the disulfide bridge would be of biochemical utility. For example, the disulfide-dependent redox protein thioredoxin (and glutaredoxin) has many physiological functions in mesophilic organisms and is typically reduced by NADPH-specific oxidoreductases (*63*). The genome sequence of *Pf* (http://comb5-156.umbi.umd.edu/) contains three homologues of thioredoxin and one of NADPH:thioredoxin oxidoreductase, as well as homologues of several thioredoxin-dependent enzymes (but not the spinach-type Fd:thioredoxin reductase). Hence, the need for direct electron transfer from Fd to a disulfide-containing, thioredoxin-like system is not obvious. On the other hand, this Fd is the only 4Fe- (or 8Fe-) type Fd present in the genome, and so multiple physiological functions are possible. The recent findings of a thioredoxin-like protein that contains an FeS center in place of the expected disulfide (*64*) and of a disulfide bond that stabilizes the cluster in a [2Fe-2S] Fd (*64*, *65*) show that much remains to be understood about the nature, function, and evolution of these two types of redox center. Attempts to determine the number and types of thioredoxin-related proteins in *Pf* are currently in progress.

The present results suggest several parallel avenues for future NMR work. First, we have shown that, for *Pf* Fd, neither the average structure nor the thermodynamics of the *S*- ⇔ *R*-disulfide orientational equilibrium are significantly perturbed by its addition of up to ~30% methanol (*39*). The addition of the cryosolvent, however, allows the use of temperatures to −20 °C, where it may be expected that several of the peptide NHs that severely broaden above 30 °C may be resolved and their distinct environments interrogated. Next, comparison of NMR spectral parameters for *Pf* Fd with intact and cleaved disulfide bond had shown that the peptide NH chemical shifts differ significantly in the two forms only for those residues whose NH exhibited severe line broadening due to the *S*- ⇔ *R*-disulfide interconversion (*20*). The difference in chemical shifts, as well as the excess line broadening, tends toward zero near 100 °C, where it is now known the *R*-disulfide orientation dominates (*20*). Hence, the *Pf* Fd with cleaved disulfide and *Pf* Fd with disulfide at very elevated temperature [or mutated Cys21(***V***) and/or Cys48(***VI***)] are suggested to resemble the structure of one (the *R*-disulfide) of the two interconverting structures of *Pf* Fd with an intact disulfide bond (*20*). An ambient temperature the solution structure of the homogeneous Fd with abolished disulfide and the redetermination of the present structure near 100 °C are high priorities and under current study. Last, the consequence of Trp2 and Tyr46 mutation for both solution NMR structure and disulfide reducibility should provide additional insight into the link between specific interaction in the Fd and the stabilization/destabilization of specific secondary structural elements. Each of these three areas will be systematically explored in the future.

ACKNOWLEDGMENT

The authors are indebted to Drs. Q. Teng and C. M. Gorst for generating some of the experimental NMR data.

SUPPORTING INFORMATION AVAILABLE

Five figures (schematic of H-bonds for β-sheets A and B in *Pf* and *Tm* Fd, Ramachandran plot, separate superposition of whole structure, cluster, and β-sheet B for *S*- and *R*-disulfide orientation) and five tables (long and short mixing time NOESY, steady-state NOE, paramagnetic relaxation, and H-bonds) of constraints used in structue. This material is available free of charge via the Internet at http://pubs.acs.org.

REFERENCES

1. Cammack, R. (1993) *Adv. Inorg. Chem. 38*, 281−322.
2. Beinert, H., Holm, R. H., and Münck, E. (1997) *Science 277*, 653−659.
3. Howard, J. B., and Rees, D. C. (1991) *Adv. Protein Chem. 42*, 199−280.
4. Sticht, H., and Rösch, P. (1998) *Prog. Biophys. Mol. Biol. 70*, 95−136.
5. Bertini, I., Ciurli, S., and Luchinat, C. (1995) *Struct. Bonding 83*, 2−53.
6. Bertini, I., Luchinat, C., and Rosato, A. (1999) *Adv. Inorg. Chem. 47*, 251−282.
7. Jensen, G. M., Warshel, A., and Stephens, P. J. (1994) *Biochemistry 33*, 10911−10924.
8. Mouesca, J. M., Chen, J. L., Noodleman, L., Bashford, D., and Case, D. A. (1994) *J. Am. Chem. Soc. 116*, 11898−11914.
9. Stephens, P. J., Jollie, D. R., and Warshel, A. (1996) *Chem. Rev. 96*, 2491−2513.
10. Swartz, P. D., Beck, B. W., and Ichiye, T. (1996) *Biophys. J. 71*, 2958−2969.
11. Blake, P. R., Park, J.-B., Bryant, F. O., Aono, S., Magnuson, J. K., Eccleston, E., Howard, J. B., Summers, M. F., and Adams, M. W. W. (1991) *Biochemistry 30*, 10885−10891.
12. Macedo-Ribeiro, S., Martins, B., Pereira, P., Buse, G., Huber, R., and Soulimane, T. (2001) *J. Biol. Inorg. Chem. 6*, 663−674.
13. Macedo-Ribeiro, S., Darimont, B., Sterner, R., and Huber, R. (1996) *Structure 4*, 1291−1301.
14. Aono, S., Bentrop, D., Bertini, I., Donaire, A., Luchinat, C., Niikura, Y., and Rosato, A. (1998) *Biochemistry 37*, 9812−9826.
15. Day, M. W., Hsu, B. T., Joshua-Tor, L., Park, J.-B., Zhou, Z. H., Adams, M. W. W., and Rees, D. C. (1992) *Protein Sci. 1*, 1494−1507.
16. Pfeil, W., Gesierich, U., Kleemann, G. R., and Sterner, R. (1997) *J. Mol. Biol. 272*, 591−596.
17. Sticht, H., Wildegger, G., Baumann, B., Bentrop, D., Darimont, B., Sterner, R., Sutter, M., Haehnel, W., and Rösch, P. (1995) in *Proceedings of the International Conference on Molecular Structural Biology* (Kungl, A. J., Andrew, P. J., and Schreiber, H., Eds.) pp 73−82.
18. Sticht, H., Wildegger, G., Bentrop, D., Darimont, B., Sterner, R., and Rösch, P. (1996) *Eur. J. Biochem. 237*, 726−735.
19. Teng, Q., Zhou, Z. H., Smith, E. T., Busse, S. C., Howard, J. B., Adams, M. W. W., and La Mar, G. N. (1994) *Biochemistry 33*, 6316−6326.
20. Wang, P.-L., Calzolai, L., Bren, K. L., Teng, Q., Jenney, F. E., Jr., Brereton, P. S., Howard, J. B., Adams, M. W. W., and La Mar, G. N. (1999) *Biochemistry 38*, 8167−8178.
21. Wang, P. L., Donaire, A., Zhou, Z. H., Adams, M. W. W., and La Mar, G. N. (1996) *Biochemistry 35*, 11319−11328.
22. Fujii, T., Hata, Y., Oozeki, M., Moriyama, H., Wakagi, T., Tanaka, N., and Oshima, T. (1997) *Biochemistry 36*, 1505−1513.
23. Jaenicke, R., Schurig, H., Beaucamp, N., and Ostendorp, R. (1966) *Adv. Protein Chem. 48*, 181−269.
24. Vogt, G., Woell, S., and Argos, P. (1997) *J. Mol. Biol. 269*, 631−643.
25. Vieille, C., and Zeikus, J. G. (1996) *Trends Biotechnol. 14*, 183−190.
26. Beadle, B. M., Baase, W. A., Wilson, D. B., Gilkes, N. R., and Shoichet, B. K. (1999) *Biochemistry 38*, 2570−2576.
27. Kissinger, C. R., Sieker, L. C., Adman, E. T., and Jensen, L. H. (1991) *J. Mol. Biol. 219*, 693−715.
28. Fukuyama, K. (2001) in *Handbook of Metalloproteins* (Messerschmidt, A., Huber, R., Poulos, T. L., and Weighardt, K., Eds.) pp 543−552, John Wiley & Sons, New York.
29. Davy, S. L., Osborne, M. J., and Moore, G. R. (1998) *J. Mol. Biol. 277*, 683−706.
30. Goodfellow, B. J., Macedo, A. L., Rodrigues, P., Moura, I., Wray, V., and Moura, J. J. G. (1999) *J. Biol. Inorg. Chem. 4*, 421−430.
31. Sieker, L. C., and Adman, E. T. (2001) in *Handbook of Metalloproteins* (Messerschmidt, A., Huber, R., Poulos, T. L., and Wieghardt, K., Eds.) pp 574−592, John Wiley & Sons, New York.
32. Stout, C. D. (2001) in *Handbook of Metalloproteins* (Messerschmidt, A., Huber, R., Poulos, T. L., and Wieghardt, K., Eds.) pp 560−573, John Wiley & Sons, New York.
33. Kim, C., Brereton, P. S., Verhagen, F. J. M., and Adams, M. W. W. (2001) *Methods Enzymol. 334*, 30−45.
34. Busse, S. C., La Mar, G. N., Yu, L. P., Howard, J. B., Smith, E. T., Zhou, Z. H., and Adams, M. W. W. (1992) *Biochemistry 31*, 11952−11962.
35. Donaire, A., Gorst, C. M., Zhou, Z. H., Adams, M. W. W., and La Mar, G. N. (1994) *J. Am. Chem. Soc. 116*, 6841−6849.
36. Calzolai, L., Gorst, C. M., Zhao, Z.-H., Teng, Q., Adams, M. W. W., and La Mar, G. N. (1995) *Biochemistry 34*, 11373−11384.
37. Calzolai, L., Zhou, Z. H., Adams, M. W. W., and La Mar, G. N. (1996) *J. Am. Chem. Soc. 118*, 2513−2514.
38. Gorst, C. M., Zhou, Z. H., Ma, K. S., Teng, Q., Howard, J. B., Adams, M. W. W., and La Mar, G. N. (1995) *Biochemistry 34*, 8788−8795.
39. Webba da Silva, M., Sham, S., Gorst, C. M., Calzolai, L., Brereton, P. S., Adams, M. W. W., and La Mar, G. N. (2001) *Biochemistry 40*, 12575−12583.
40. Yu, L., Faham, S., Roy, R., Adams, M. W. W., and Rees, D. C. (1999) *J. Mol. Biol. 286*, 899−914.
41. Gorst, C. M., Yeh, Y. H., Teng, Q., Calzolai, L., Zhou, Z. H., Adams, M. W. W., and La Mar, G. N. (1995) *Biochemistry 34*, 600−610.
42. Bertini, I., Luchinat, C., and Rosato, A. (1996) *Prog. Biophys. Mol. Biol. 66*, 43−80.
43. Goodfellow, B. J., and Macedo, A. L. (1999) in *Reports on NMR Spectroscopy*, pp 119−177, Academic Press, London.
44. Huber, J. G., Moulis, J.-M., and Gaillard, J. (1996) *Biochemistry 35*, 12705−12711.
45. Zhou, Z. H., and Adams, M. W. W. (1997) *Biochemistry 36*, 10892−10900.
46. Brereton, P. S., Verhagen, F. J. M., Zhou, J. H., and Adams, M. W. W. (1998) *Biochemistry 37*, 7351−7362.
47. La Mar, G. N., and de Ropp, J. S. (1993) *Biol. Magn. Reson. 18*, 1−78.
48. Banci, L., Bertini, I., and Luchinat, C. (1991) *Nuclear and Electron Relaxation*, VCH, Weinheim, FRG.
49. Donaire, A., Zhou, Z. H., Adams, M. W. W., and La Mar, G. N. (1996) *J. Biomol. NMR 7*, 35−47.
50. Richardson, J. S. (1981) *Adv. Protein Chem. 34*, 167−330.
51. Busse, S. C., La Mar, G. N., and Howard, J. B. (1991) *J. Biol. Chem. 266*, 23714−23723.
52. La Mar, G. N. (2001) in *Methods in Enzymology* (Adams, M. W. W., and Kelly, R. M., Eds.) pp 351−389, Academic Press, San Diego.
53. Eidsness, M. K., Richie, K. A., Burden, A. E., Kurtz, D. M. J., and Scott, R. A. (1997) *Biochemistry 36*, 10406−10413.
54. Fiala, G., and Stetter, K. O. (1986) *Arch. Microbiol. 145*, 56−61.
55. Huber, R., Langworthy, T. A., König, H., Thomm, M., Woese, C. R., Sleytr, U. B., and Stetter, K. O. (1986) *Arch. Microbiol. 145*, 324−333.
56. Kress, L. F., and Laskowski, M., Sr. (1967) *J. Biol. Chem. 242*, 4925−4929.
57. Otting, G., Liepinsh, E., and Wüthrich, K. (1993) *Biochemistry 32*, 3571−3582.
58. Vallee, B. L., and Williams, R. J. P. (1968) *Proc. Natl. Acad. Sci. U.S.A. 59*, 498−504.
59. Staples, C. R., Gaymard, E., Stritt-Etter, A. L., Telser, J., Hoffman, B. M., Schurmann, P., Knaff, D. B., and Johnson, M. K. (1998) *Biochemistry 37*, 4612−4620.
60. Duin, E. C., Madadi-Kahkesha, S., Hedderich, R., Clay, M. D., and Johnson, M. K. (2002) *FEBS Lett. 512*, 263−268.
61. Dai, S., Schwendtmayer, C., Schurmann, P., Ramaswamy, S., and Eklund, H. (2000) *Science 287*, 655−658.
62. Verhagen, M. F. J. M., Menon, A. L., Schut, G. J., and Adams, M. W. W. (2001) *Methods Enzymol. 330*, 12−25.
63. Ritz, D., and Beckwith, J. (2001) *Annu. Rev. Microbiol. 55*, 21−48.
64. Yeh, A. P., Chatelet, C., Soltis, S. M., Kuhn, P., Meyer, J., and Rees, D. C. (2000) *J. Mol. Biol. 300*, 587−595.
65. Meyer, J., Clay, M. D., Johnson, M. K., Stubna, A., Münck, E., Higgins, C., and Wittung-Stafshede, P. (2002) *Biochemistry 41*, 3096−3108.

BI020347+